Bulletin of Engineering Geology and the Environment (2022) 81:415
https://doi.org/10.1007/s10064-022-02914-6

ORIGINAL PAPER

Investigating the effect of hematite additive on the performance of clay barriers for radioactive waste disposals

Abbas Salati[1] · Hajar Share Isfahani[1] · Mohammad Ali Roshanzamir[1] · Amin Azhari[2]

Received: 4 August 2021 / Accepted: 31 August 2022

Abstract

The radiation shielding performance of bentonite clay as the main component of the landfill liners is investigated using hematite powder as an additive. For this, theoretical and experimental methods have been used to examine different mixtures of hematite powder and bentonite clay, including pure bentonite, and bentonite with 15, 30, and 45% of hematite powder. Energy-dispersive X-ray (EDS) and scanning electron microscopy (SEM) experiments are undertaken to better understand and analyze bentonite and hematite from a chemical perspective. To evaluate the radiation shielding performance of the mixtures, the linear attenuation coefficient is calculated and simulated employing the XCOM database and MCNP code, respectively. The results are then compared with the experimental approach of radiation permeation by a NaI (Tl) detector which were in good agreement. The hydraulic permeability tests have been also conducted to ensure that the mixtures meet the requirement according to the EPA standard. The results revealed that with increasing the additive percentage the attenuation coefficient grows linearly; however, the hydraulic permeability increases simultaneously. The bentonite with 45% hematite powder outperformed other compounds in providing 30 and 50% improvement in gamma-ray radiation shielding and a 25% and 17% decrease in both TVL and HVL values, at the energy levels of 1173 and 1332 keV, respectively.

Keywords Sodium bentonite · Hematite · Radiation shielding · Nuclear waste management · Hydraulic permeability

Introduction

Nowadays, with the advancement of technology, countries around the world have become interested in various uses of nuclear energy in industries such as agriculture, medicine, and industry (Rahman et al. 2011; Damla et al. 2012; Singh et al. 2017; Elmahroug et al. 2014). One of the challenges is radioactive waste management due to difficulties such as environmental hazards, negative genetic effects, cancer, cell destruction, headache, and vomiting (Akman et al. 2019a, b; Poltabtim et al. 2018; Singh et al. 2018a, b). These negative effects occur due to hazardous radiation such as gamma, beta, and neutrons emitted from nuclear waste. Therefore, it must be controlled by one of the excretion methods. However, most of the waste is low-level radioactive waste (LLRW). Therefore, proper and safe disposal of these substances is one of the most significant concerns. One of the most widely used methods of waste management and disposal is surface landfilling and storage (Saling 2001; Lersow and Waggitt 2020). However, the use of this method carries risks such as the possibility of groundwater and surface water leaking to landfills and, consequently, radiation outside the landfill. To overcome these problems, a protective layer is used around the landfill. To construct this shielding layer, various materials such as lead and heavy concrete are commonly used materials with high atomic numbers. However, due to the toxicity of lead (Lansdown and Yule 1986; Yue et al. 2009; Flora et al. 2012; Wani et al. 2015; Billen et al. 2019) or the environmental pollution of cement (Uwsau et al. 2014; Li et al. 2020), researchers are looking for alternatives. Bentonite is one of the available, cheap, sealing, and durable materials (Omotoyinbo and Oluwole 2008; Adegoka 1980). Therefore, bentonite can be considered a suitable alternative liner for radioactive disposal landfills, due to its two properties of shielding and controlling hazardous rays (Koch 2002). Bentonite is recently used in Europe and the USA as a radiation shielding layer (Lee and Tank 1985; Pusch et al. 2013). There is a large number of studies on the properties of radiation shielding

✉ Hajar Share Isfahani
hajarshare@iut.ac.ir

[1] Department of Civil Engineering, Isfahan University of Technology, Isfahan 84156-83111, Iran

[2] Department of Mining Engineering, Isfahan University of Technology, Isfahan 84156-83111, Iran

Published online: 14 September 2022

by various materials. The following presents the studies conducted on five general groups of materials, namely heavy concrete, polymers, rocks, elements, and soil.

Heavy concrete is consistent with the Beer-Lambert theory and has attracted the attention of researchers, due to its high density. Abdo et al. (2002), investigated the properties of gamma and neutron absorption by barite concrete and compared the results with the XCOM code (Abdo et al. 2002). Ristinah et al. (2011) made heavy concrete using steel fibers to increase the density and the gamma-ray absorption by increasing the density, where their goal was stability in the mechanical properties of concrete. It was concluded that fiber concrete with steel fibers has the potential for radiation shielding (Ristinah et al. 2011). Nikbin et al. (2019) also investigated the properties of gamma-ray absorption by heavy concrete containing titanium dioxide nanoparticles. In this research, 60 cobalt and 137 cesium sources have been used to produce radiation with intensities of 662, 1173, and 1332 keV (Nikbin et al. 2019). El-Sayed (2021) investigated the mechanical and radiation protection properties of heavy concrete including magnetite aggregate, cement, rice husk ash, polyethylene, boric acid, nano-silica, and water reducer. The results show that magnetite concrete containing 3% polyethylene is the best mixture for radiation shielding (El-Sayed 2021).

A study by Nambiar and Yeow (2012) on the use of five different types of polymer composites used as radiation shields is conducted, which emphasizes the preservation of features such as efficiency, lightness, cost-effectiveness, and flexibility. Polymer composites were reinforced with various micro- or nano-materials (Nambiar and Yeow 2012). Mann et al. (2015) investigated the physical parameters and behavior of some polymeric materials exposed to gamma-rays, including bone-equivalent plastic, polyvinyl chloride, air-equivalent plastic, radio chromic dye film (nylon base), polyethylene terephthalate (mylar), polymethyl methacrylate (PMMA), and concrete. They examined the mass attenuation coefficient of the samples by WinXCom software. According to the results of mass attenuation coefficient and equivalent atomic number, it was found that polyvinyl chloride has the maximum ability to protect against gamma-rays for the energy range of 10 to 110 keV, among the selected samples and concrete (Mann et al. 2015). Kacal et al. (2019) investigated the absorption of gamma and neutron radiation by eight different polymer samples. These examples included polymers such as polyamide (PA-6), polyacrylonitrile (PAN), polyvinylidene chloride (PVDC), polyaniline (PANI), polyethylene terephthalate (PET), polyphenylene sulfide (PPS), polypyrrole (PPy), and polytetrafluoroethylene (PTFE). The experimental linear attenuation coefficient values are compared with the theoretical data of the WinXCom database using a high-resolution germanium detector and various radioactive sources in the energy range of 81 to 1333 keV. PTFE was found to have the highest density and, therefore, the highest linear attenuation coefficient (Akman et al. 2019a, b). Mahmoud et al. (2020) investigated the protective properties of polyvinyl chloride (PVC) along with various fabricated hematite- and chalcocite-based PVCs. Here, the mass attenuation coefficient for various samples was calculated using the MCNP code and the results have been obtained with the values calculated using XCOM software at different energy levels. The results showed that the addition of hematite and chalcocite increased the mass attenuation coefficient of polyvinyl chloride polymers. The highest mass attenuation coefficient was obtained for polyvinyl chloride polymer composite with 31% chalcocite (Mahmoud et al. 2020).

Awadallah and Imran (2007) compared the shielding properties of limestone, brick, and concrete with a high purity germanium detector. The samples were also irradiated with gamma-rays with different energy levels. A 10-cm brick is able to block 60% of gamma radiation with an energy level of 1461 keV. Seven-cm-thick limestone stops 75% of gamma-rays with an intensity of 662 keV, while a medium-thick (7 cm) brick stops about 60% for an energy level of 662 keV (Awadallah and Imran 2007). Mann et al. (2012) inspected several types of rock types and construction materials widely used in India in terms of radiation protection properties. These include soil from Bathinda, Punjab, India (S1); soil from Muktsari in Punjab, India (S2); dolomite (S3); gypsum (S4); igneous rock (S5); and limestone (S6). The results showed that soil samples S1 and S2 were the best shielding material against the gamma-rays in the energy range of 0.015 to 15 MeV. The protective effect of all samples is the same in the energy range of 0.3 to 3 MeV. However, the S4 sample acts as a suitable shielding material for deep penetration in the energy range of 3–15 MeV (Maan et al. 2012). The physical properties of some ores against gamma-rays were investigated by Oto et al. (2015). In this study, the linear attenuation coefficient of barite, magnetite, limonite, hematite, and serpentine minerals are investigated emitting photons with energy levels of 383, 356, 312, 276, and 81 keV released from barium 133 and photons with energy levels of 444, 344, 121, 244, and 778. The emitted photon from europium 152 was determined using a high purity germanium (HPGe) detector. Barite has the highest linear attenuation coefficient. Therefore, it is superior to other samples in terms of shielding properties. In general, the results show that barite and magnetite were found more effective as protective materials against gamma-rays (Oto et al. 2015). Obaid et al. (2018) evaluated seven rock types, namely olivine basalt, green marble, jet black granite, black granite, Cuddapah limestone, white marble, and pink marble for radiation shielding. In this experiment, cobalt 60, barium 133, sodium 22, cesium 137, and manganese 54 sources were used to generate gamma-rays in the NaI (Tl) detector. The results were compared with the simulation results with XCOM software and the

MCNP code where a reasonable agreement was observed. The results showed that the values of linear attenuation coefficient in pink marble are maximum whereas these values were minimum in black granite (Obaid et al. 2018). Alorfi et al. (2020) examined four rock samples from East, West, South, and North Saudi Arabia with various geomechanical characteristics. The samples were then compared with concrete and brick. The WinXCom computer program was used to calculate the half-layer absorption coefficient and linear/mass attenuation coefficient. Stone samples are better protective materials for low gamma-ray energy (medium energy for diagnostic radiology applications), while concretes and bricks are better for nuclear medicine diagnostic energies. RW rock samples have the best protective properties at energy 22, 32, 42, and 62 keV and of course with the highest performance at 22 keV; therefore, stone samples can replace the materials that are now used to build nuclear diagnostic centers and radiological facilities due to their properties and cheap price (Alorfi et al. 2020). A study on the combination of different percentages of lead and tin metal alloys was conducted to examine the performance of gamma-ray shielding (Kaur et al. 2016). Lead and tin metal alloys were prepared in different compositions and then various physical parameters such as effective atomic number, electron density, and the average free path for the energy range from 1 keV to 100 GeV were calculated. The various compounds made in this experiment include 90% tin with 10% lead, 30% tin with 70% lead, 50% lead with 50% tin, and vice versa. The results show that among the selected alloys, the maximum effective atomic number in the whole energy region belongs to alloys with 90% lead with 10% tin. However, the minimum effective atomic number values were observed at 90% tin along with 10% lead (Kaur et al. 2016).

Singh et al. (2017) investigated the protective effect of lead and copper metal alloys. The combinations of these two metal alloys are prepared based on the equation of $x\mathrm{Pb} - (1 - x)$ Cu where x changes from 0.1 to 0.9 with an incremental rate of 0.1. Detector (NaI) Tl physical properties and protection parameters against gamma-rays were examined in terms of density, mass attenuation coefficient, free path average, absorption half-thickness, eleventh absorption layer thickness, effective atomic number, effective electron number, and radiation protection efficiency. Among the selected alloys, the combinations of 90% lead with 10% copper with maximum specific gravity, linear/mass attenuation coefficient, and thus the best combination for use as a radiation absorber were investigated (Singh et al. 2018a, b). Agar et al. (2019) have investigated the properties of alloys containing lead and silver against radiation emission. In this study, four samples of alloys with different mixing percentages at different photon energies between 81 and 1333 keV were irradiated using an HPGe detector, and the mass attenuation coefficients were measured in addition to the experimental results with simulation results including WinXCom software and the MCNP code. The 75% lead-25% silver alloy sample with the maximum radiation protection efficiency was found to be 53% for the energy level of 81 keV and a minimum thickness of the absorption half-layer compared to other alloys (Agar et al. 2019). Levet et al. (2020) investigated the radiation absorption properties of iron and boron alloys for samples with different percentages of alloys with the formula $\mathrm{Fe}(100 - x)\mathrm{B}(x)$, where x is the alloy percentage (between 1 and 20). In this research, radioactivity sources including americium 241, barium 133, and europium 152 have been used in Ultra Ge detector where physical parameters including mass attenuation coefficient, absorption half-layer thickness, and the effective atomic number were calculated. The results were then simulated using the WinXCom database. Iron powder with 95.99% purity and boron powder with 99% purity were used to create the sample. The results show that iron and boron alloy containing 20% boron have the highest values of absorption half-layer thickness compared to other samples (Levet et al. 2020).

Ciaravella et al. (2004) investigated the effect of X-ray radiation on pure deoxyribonucleic acid (DNA) and DNA impregnated with clay (montmorillonite and kaolinite). In this study, DNA samples were exposed to X-rays under different intensities and for different durations. The biological deformation technique was used to estimate the extent of DNA damage. It is obvious that the amount of damage varies depending on the intensity of the radiation. The results showed that DNA impregnated with clay was found to be several times more resistant to radiation than pure DNA (Ciaravella et al. 2004). Akkurt and Canakci (2011) investigated the properties of boron in combination with clay to protect against radiation. They have studied the photon attenuation coefficient of clay using different percentages of boron, i.e., 5 to 30%, in order to investigate the mixture application in the disposal of radioactive waste. In this study, five types of clay samples with different percentages of boron were tested using the (NaI) Tl detector at energy levels of 662, 1173, and 1332 keV, utilizing cesium sources of 137 and cobalt 60. By measuring the linear attenuation coefficient, it was found that boron in clay increases the coefficient. It can be concluded from this study that boron is effective for radiation protection (Akkurt and Canakci 2011). Mann et al. (2016) evaluated the radiation protection properties of light clay. The initial compositions of clay bricks with fly ash were investigated using energy-dispersive X-ray fluorescence spectrometry (EDXRF) spectroscopy and the samples were compared with concrete samples (witness sample). Two variable parameters were examined, the intensity of radiation energy and the ash percentage. In this experiment, the intensity of radiation energy is 1173, 661, and 1332 keV, and samples of pure clay and clay with ash in percentages of

10, 20, 30, 40, and 50% have been exposed to gamma-rays. The results showed that the multilayer exterior walls made of these bricks could effectively reduce the transmission of gamma-rays (Mann et al. 2016). Share Isfahani et al. (2019) studied the effect of clay modified by barite to improve the radiant performance and maintain the low hydraulic permeability of the clay. In this research, HPGe was used to measure the linear and mass attenuation coefficients at energy levels of 662, 1173, and 1332 keV. Radiation attenuation coefficients were simulated using the MCNP code and XCOM database which were in good agreement with the experimental results. In general, the results showed that the combination of bentonite with 40% barite powder can form a reliable mixture against radiation shielding and hydraulic permeability (Isfahani et al. 2019). Asal et al. (2021) examined the radiation shielding performance of different percentages of ceramic as an additive for bentonite. They concluded that the mass and linear attenuation coefficients of the prepared mixtures vary between 0.238 and 0.443 $cm^2\ g^{-1}$ and between 0.479 and 1.06 cm^{-1}, respectively, depending on their thicknesses. El-sharkawy et al. (2022) studied new nanocomposites, based on bentonite clay and bismuth oxide nanoparticles (Bi2O3 NPs), as a non-toxic nano-additive. They used the theoretical XCOM procedure, and experimental method using a NaI (Tl) scintillation detector. It was found that the γ-ray shielding properties were improved by increasing the loading of bismuth oxide nanoparticles. Ultimately, the nanocomposite specimen, containing 40.0 wt% Bi2O3 NPs, was characterized to experience the highest linear attenuation coefficient value.

Investigating the shielding performance against gamma-rays with the help of clay composites with polyethylene was conducted in the field of gamma radiation protection. Olukotun et al. (2020) made clay-polyethylene composites with seven different types of low-density recycled polyethylene, containing the weight percentage of polyethylene, in which the composite density varies between 1.34 and 2.33 g/cm^3. The results show that the gamma-ray shielding performance for composites increases by reducing the percentage of polyethylene (density reduction) in the clay mixture. However, the protective effect of the composites was significant, which indicates the suitability of composites for gamma-ray protective applications (Olukotun et al. 2020).

Considering the suitable properties of bentonite for use in low-level landfills, this study aimed to increase the gamma-ray shielding performance of bentonite mixed with different percentages of hematite powder while maintaining the hydraulic permeability coefficient within the allowable range. An experimental approach along with theoretical and simulation methods is used for the analyses.

Materials and methods

Materials

Bentonite is a type of clay that has more than 95% montmorillonite and the remaining components are quartz, feldspar, smectite, illite, kaolinite, calcite, chlorite, and pyrite (Cokca and Yilmaz 2004; Akgun et al. 2017). Bentonite has two types of sodium and calcium, where sodium bentonite was used in this study due to extensive applications used in cases in the field and the high swelling capacity of sodium bentonite with lower hydraulic permeability (Cui 2017). Moreover, due to the significantly low hydraulic permeability (between 1×10^{-11}and1×10^{-9}) and the importance of this feature for landfill cover, bentonite had a larger share compared to other soils (Swiss Standard 1999). The grading curve of the sodium bentonite used in this study obtained from the hydrometric experiment is presented in Fig. 1.

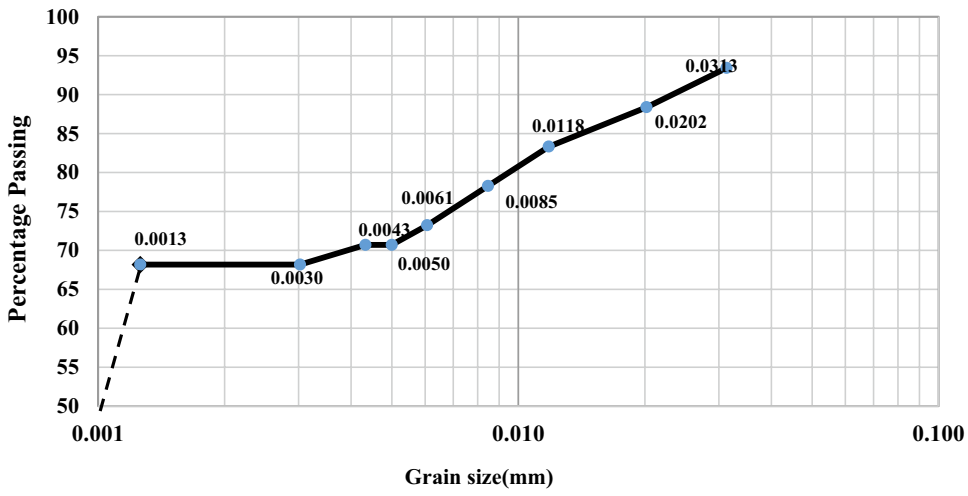

Fig. 1 Sodium bentonite grading curve

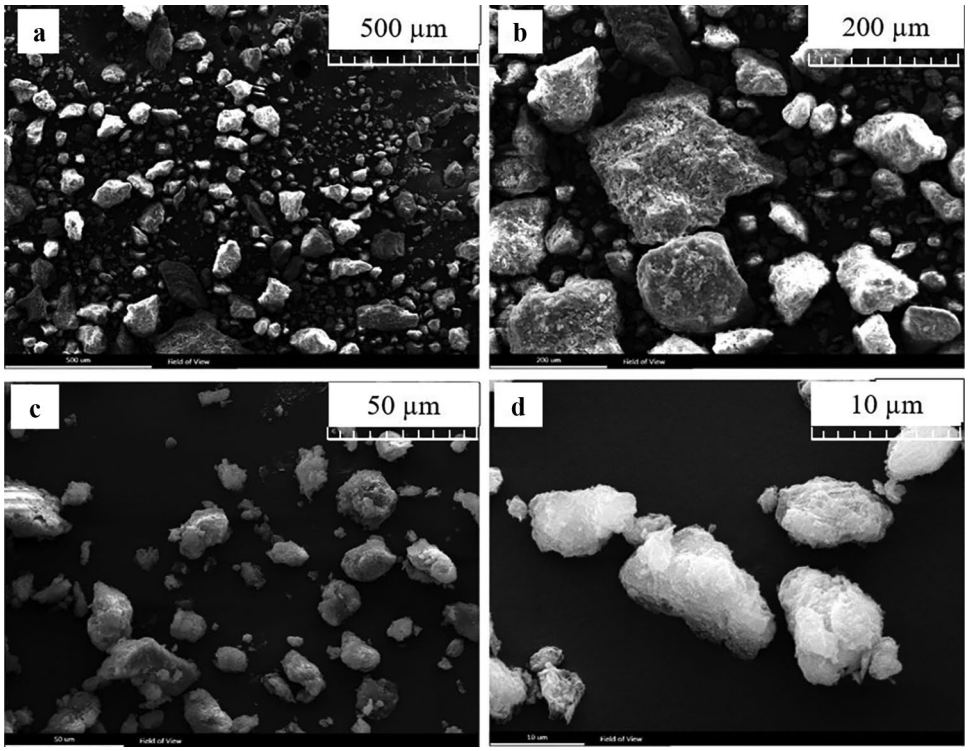

Fig. 2 Scanning electron microscope images for sodium bentonite powder

Ordinary hematite (Fe2*O*3) is a mineral rich in iron ore and has capable of absorbing radiation. It is common to find hematite in hydrothermal veins and magmatic rocks (Kavaz 2019). Pure hematite has a Moore hardness of between 5.5 and 6.5 and a specific gravity of between 4.9 and 5.5 g/cm^3 (Gencel 2011; Gencell et al. 2011). However, the specific gravity of hematite ore can be between 3.2 and 4.3 (Gencel 2011). The hematite used in this research was initially in the form of rock lumps prepared from the mines of central Iran, which were crushed particles that passed through the sieve of grade 10 used.

The chemical analysis was performed. The soil microstructure for bentonite and hematite was examined via scanning electron microscopy (SEM) with four different scales and energy scattering spectroscopy (EDS). The results of the SEM analysis for bentonite and hematite powder are shown in Figs. 2 and 3, respectively. The results of the energy scattering spectroscopy are presented in Table 1.

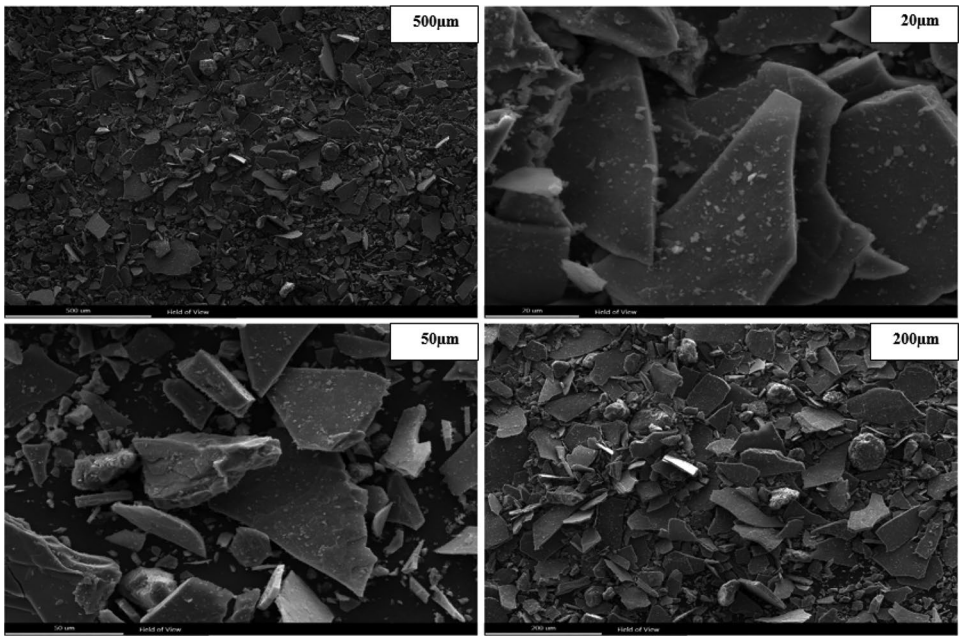

Fig. 3 Scanning electron microscope images for hematite powder

Table 1 Chemical analysis of bentonite in pure form and with different percentages of hematite powder

Atomic percentage									Sample (index)
Fe	Ca	K	Cl	Mg	Na	Si	Al	O	
2/57	0/39	0/59	0/86	0/91	2/47	45/42	7/83	38/97	BS
15/66	0/52	0/5	0/73	0/77	2/10	38/71	6/65	34/35	BSH15
28/76	0/64	0/39	0/6	0/63	1/73	32	5/48	29/73	BSH30
41/86	0/76	0/32	0/47	0/5	1/36	25/28	4/3	25/11	BSH45

It can be seen from Figs. 2 and 3 that hematite powder has a denser structure than bentonite powder. The structure of hematite powder is layered, while the structure of hematite powder is oval.

Table 1, which is based on information from the SEM test, shows that the most important elements in sodium bentonite are silicon (Si), oxygen (O), and aluminum (Al), while most of the hematite powder is composed of iron (Fe) and oxygen (O).

Sample preparation

To perform gamma-ray penetration and hydraulic permeability tests, a combination of sodium bentonite and hematite powder is placed in a dryer (oven) at 80 °C for 48 h. Dry mixtures sit in lab condition for 4 h to adapt to the ambient temperature and cool down. To measure the linear attenuation coefficient (μ), the desired percentage of bentonite and hematite powder is mixed in the optimum moisture content. The mixture is then poured into three PVC cylindrical molds with different heights and the same diameter. Figure 4 illustrates the prepared samples with heights of 2, 4, and 8 cm and the used mold for the sample preparation.

To prepare the specimen for the constant water load hydraulic permeable test, the preparation process is the same as before, but we consider the height of the sample to be half the height of the test mold because the free swelling index test shows that bentonite will swell by about 25% after saturation.

Radiation shielding test

The linear attenuation coefficient (μ) is considered to assess the gamma-ray absorption properties of the material. In this research, μ is calculated using both laboratory and theoretical approaches. The linear attenuation coefficient in the laboratory has been measured by a NaI (Tl) detector and theoretically calculated by the XCOM database along with the MCNP simulation code.

Theory and experimental radiation shielding test

To calculate the linear attenuation coefficient in the laboratory, the NaI (Tl) detector was used. Gamma-rays were emitted from a cobalt 60 source at two commonly used energy levels of 1173 and 1332 keV. This detector generally has five parts: the energy source, the shielding lead plate, the specimen station, the scintillation detector, and the plotting system. The test setup to determine the linear attenuation coefficient with the NaI (Tl) detector is shown in Fig. 5. Two steel collimators are used at the top and bottom of the sample. To calculate the linear attenuation coefficient, the gamma-ray intensity is detected on the scintillation detector without (N_0) and with sample (N). As a result, at both energy levels, $\ln\frac{N_0}{N}$ is plotted in terms of

Fig. 4 The prepared samples with bentonite base with 15, 30, and 45% of hematite powder in heights of 2, 4, and 6 cm

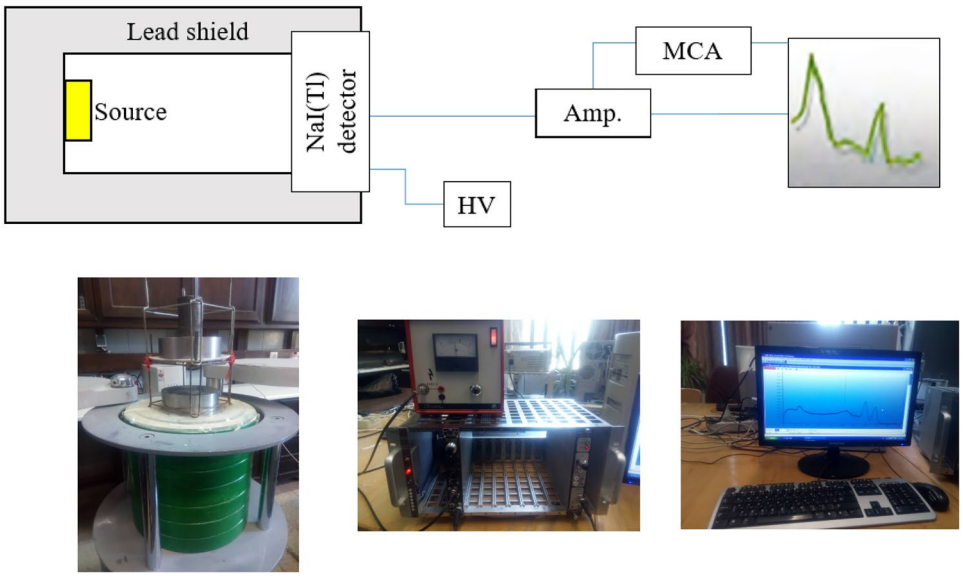

Fig. 5 Schematic view and image of the test setup to determine the linear attenuation coefficient with the NaI (Tl) detector

sample thickness (t). The slope of the diagram indicates the linear attenuation coefficient (μ) of the specimens.

When a gamma-ray passes through a soil sample with a thickness of t (in centimeters), the photons are transmitted according to the Lambert–Beer law as follows:

$$I = I_0 \exp(-\mu t) \tag{1}$$

where I_0 is the initial gamma-ray intensity, I is the gamma-ray intensity after attenuation through a soil column at height t (cm), and $\mu\left(cm^{-1}\right)$ is the linear attenuation coefficient of the soil.

The linear attenuation coefficient can be expressed by Eq. 2 as follows:

$$\mu = \mu_S \rho \tag{2}$$

where μ_S is the attenuation coefficient of a mass that has a unit of surface area on force and ρ is the density of a sample that has a unit of mass on volume. Combining Eqs. 1 and 2, we will have:

$$I = I_0 \exp(-\mu_s t) \tag{3}$$

where t is the thickness of the sample and has a unit of length.

The thickness of the absorption half-layer and the average free path are important parameters for determining the protective properties of a material. The thickness of the absorption half-layer (HVL) is the thickness required for a material that can reduce the number of gamma-rays to the original half. The thickness of the absorption half-layer can be calculated using the following Eqs. (4 and 5).

$$\mathrm{HVL} = \frac{\mathrm{Ln2}}{\mu} = \frac{0.693}{\mu} \tag{4}$$

The thickness of one-tenth of the absorption layer (TVL) is another factor known as the required thickness for radiation shielding, after which the primary photons are attenuated to one-tenth.

$$\mathrm{TVL} = \frac{\ln 10}{\mu} = \frac{2.3026}{\mu} \tag{5}$$

To evaluate the obtained linear attenuation coefficient, the maximum permissible error formula should be used. Because, the numbers obtained in this method must be within the allowable range to match the simulation and laboratory results. The error is calculated from Eq. 6:

$$\Delta(\mu) = \frac{1}{t}\sqrt{\left(\ln\left(\frac{N}{N_0}\right)\right)^2 \left(\frac{\Delta t}{t}\right)^2 + \left(\frac{\Delta N}{N}\right)^2 + \left(\frac{\Delta N_0}{N_0}\right)^2} \tag{6}$$

where Δt, ΔN_0, and ΔN are the time error, number of multipurpose without sample presence, and number of multipurpose with sample presence, respectively.

Radiation shielding simulation

The Monte Carlo N-Particle (MCNP) code is a kind of random number method, which is widely used in the field of nuclear computing. To perform the calculations, the sample dimensions, physical properties, available chemical elements, and their percentage in the composition under hypothetical radiation permeability are defined to calculate the linear attenuation coefficient. The MCNP code is an effective method to investigate the interaction of radiation on existing materials (Mahdi and Kuraan 1999). The general purpose of using the MCNP code is to model the interaction of

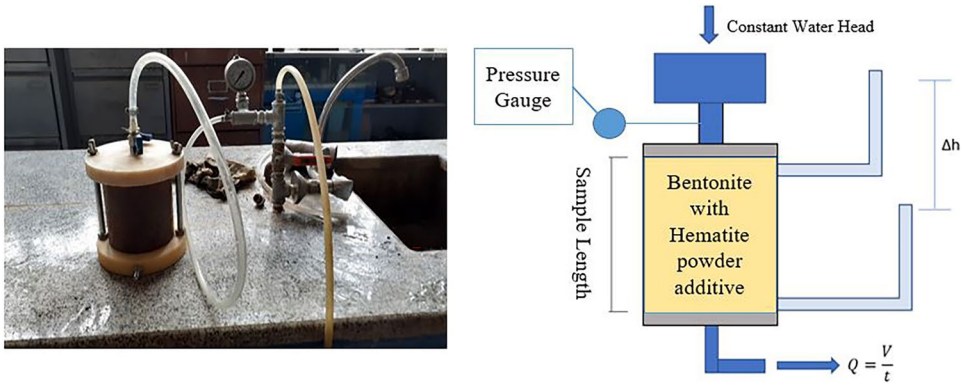

Fig. 6 Image and schematic illustration of the constant head hydraulic permeability test setup

gamma-rays and to track all particles at different energy levels. Many studies have used the MCNP code to demonstrate the effectiveness of nanoparticles for protective properties (Al-Ketan 2012; Ceglie et al. 2011).

Theoretical calculation of radiation shielding (XCOM)

The XCOM database configures the calculations based on element. The database has various information from different radiation permeability tests and, based on this information and the elemental percentage of each compound in this research, simulates and determines the linear attenuation coefficient.

The XCOM database is capable of estimating the photon cross-sections and total attenuation coefficients for elements, compounds, and mixtures at different energy levels of 1 keV to 100 GeV. The summation of the corresponding atomic constituent's quantities results in the total attenuation coefficients for mixtures and compounds. Afterward, using the XCOM database, the weighting factors defined as the weight fractions of the constituents are calculated from the chemical formula. For this, the fractions by weight of the components are defined by the user (XCOM 2010).

Hydraulic permeability test

In addition to the radiation attenuation coefficient parameter, the hydraulic permeability (K) parameter is an important property for the shielding layer materials of low-level radioactive landfills. In this study, the allowable hydraulic permeability is considered to be in the range of 1 to 3E − 10 m/sec according to the US Department of Energy (DOE) (Bonaparte et al. 2008). The permeability test was performed based on ASTM D5856-95 on different samples including pure bentonite and bentonite with 15, 30, and 45% hematite powder under constant water pressure of 300 kPa. A metal cylinder with a diameter of 110 mm and a height of 130 mm (Fig. 6) was used and the desired composition was mixed with optimal humidity and compacted in three layers with 25 weight drops in each layer. Calculate the hydraulic permeability (K) according to Darcy's law:

$$K = \frac{Q.l}{A.h.t} \tag{7}$$

where Q is the discharge volume (m^3), l is the sample length (m), A is the sample area (m^2), h is the water head (m), and t is the time (s).

Results and discussion

This study includes the results of two sets of parameters: linear attenuation coefficient (μ) and hydraulic permeability coefficient (K). These parameters are examined for four samples, namely pure sodium bentonite (BS), bentonite with 15% hematite powder (BSH15), bentonite with 30% hematite powder (BSH30), and bentonite with 45% hematite powder (BSH45). As noted earlier, bentonite is a base material in landfill covers. It is, therefore, the main component in all mixtures. Moreover, studies show that the radiation shielding characteristic of the material improves with the increase of density. As a result, the mixtures are compacted in the optimum moisture content to reach the maximum unit weight. The results of the compaction test are shown in Fig. 7.

In general, the results show that the higher the percentage of additive, the higher the density of the mixtures. This is because the density of hematite powder is about three times that of bentonite. However, this increase in the percentage of additive causes a change in the optimum humidity where BSH15, BSH30, and BSH45 have a lower optimum moisture content than BS, which is due to the significant reduction in the percentage of bentonite in these compounds (Table 2).

In this research, both experimental and simulation methods were used to calculate the linear attenuation coefficient of radiation. In the laboratory method, the detector NaI (Tl)

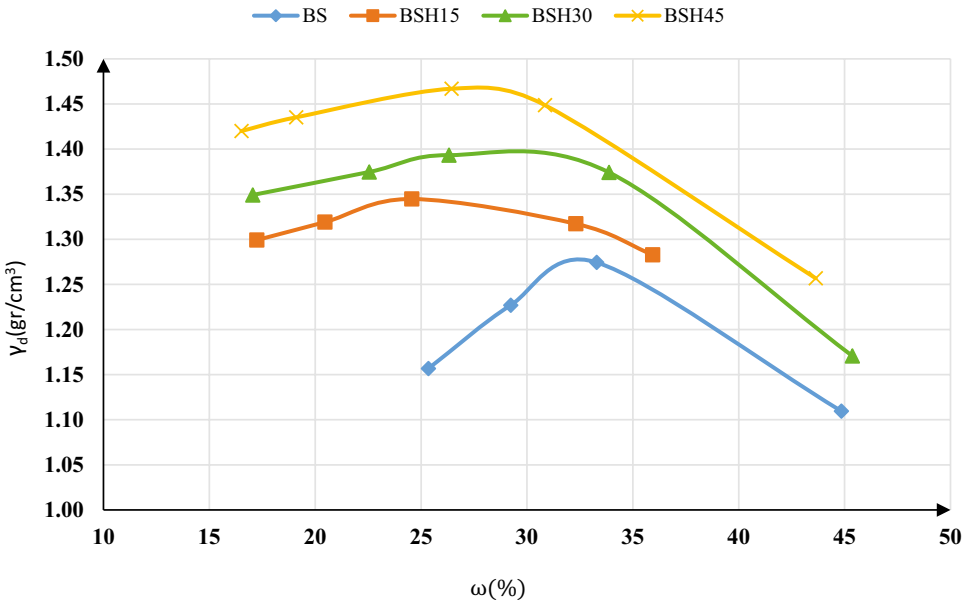

Fig. 7 Compaction curve of bentonite mixtures containing different percentages of hematite powder

is used and in the simulation methods, the MCNP code and XCOM database were employed. Figure 8 shows the results of the linear attenuation coefficient of sample types under energy levels of 1173 and 1332 keV.

Figure 8 illustrates that as the amount of hematite powder increases, the density increases. As a result, the radiation shielding properties improve. The slope of the graph represents the linear attenuation coefficient.

The linear attenuation coefficient can also be calculated via the MCNP code and the XCOM database. To use the MCNP code, the elements in the composition and the percentage of each must be specified separately. For this, the elements in each compound are defined using the X-ray fluorescence (XRF) test and are presented in Table 1. Figure 9 plots the results that were obtained from the MCNP modeling. It is evident that higher radiation shielding performance was observed for mixtures with a higher percentage of hematite powder. Hence, a higher linear attenuation coefficient was recorded. This shows that increasing the density leads to higher shielding performance of the mixtures. Also, according to this simulation, the results have good accuracy; therefore, the linear regression (R^2) of the fitted line is equal to one for all mixtures.

Table 2 Maximum dry unit weight and optimum moisture content of bentonite in pure form with different percentages of hematite powder

BSH45	BSH30	BSH15	BS	Property
1.47	1.39	1.35	1.28	Maximum dry unit weight (g/cm^3)
28	30	24	33	Optimum moisture (%)

Figure 10 shows the linear attenuation coefficient versus the maximum unit weight of the mixture. Based on the linear regression, it can be noted that there are 11% and 5% error values in attenuation coefficient relationships for energy levels of 1173 and 1332 keV, respectively. This error can be caused by the large interval percentages between adding hematite to bentonite or the use of a sodium scintillation detector instead of the high purity germanium detectors, which results in lower accuracy.

Figure 11 shows the linear attenuation coefficient versus the percentage of hematite powder additive. Based on the graph, it can be seen that there are relationships between the percentage of additive and the linear attenuation coefficient, where gamma radiation shielding performance is improved by increasing the percentage of the additive in the mixtures. The error value of the relationship between attenuation coefficient and additive percentage for energy levels of 1332 and 1173 keV is 12 and 9%, respectively. Moreover, the relationship obtained was based on the experiments and due to the low number of experiments and the large intervals between the additive percentages needs further investigation.

As the gamma-ray energy level increases, the value of the linear attenuation coefficient decreases. Increasing the energy of the rays to which the sample was exposed leads to a decrease in the amount of absorption and attenuation of gamma-rays by the shielding material. Also, increasing the thickness of the samples results in a higher value of

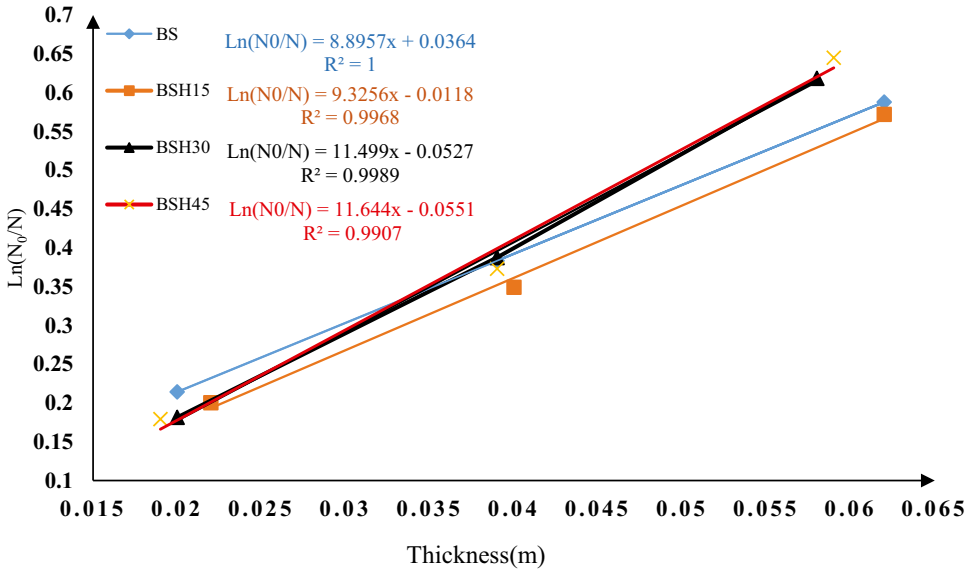

a) Energy level 1173 keV

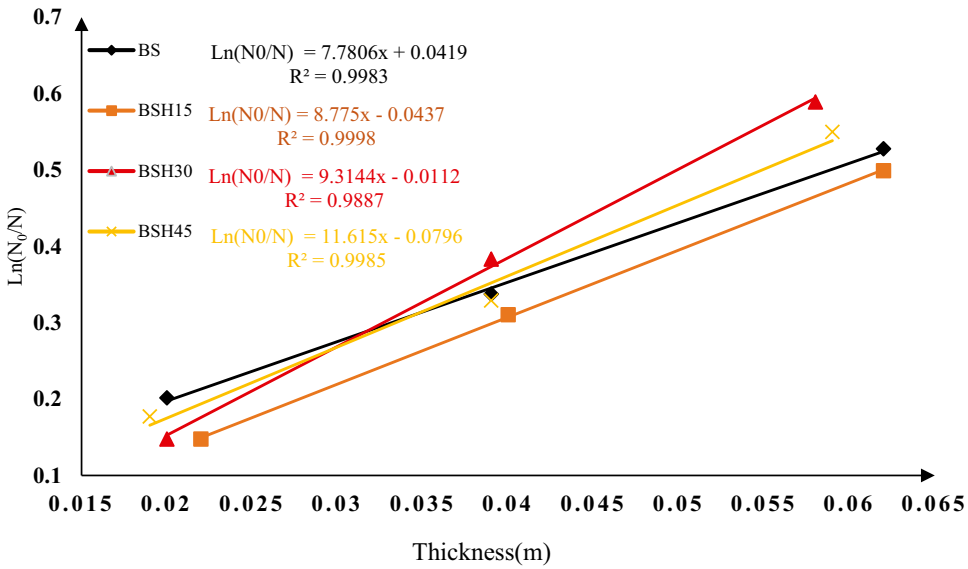

b) Energy level 1332 keV

Fig. 8 Laboratory results of the variation of $\ln\frac{N_0}{N}$ against the thickness of bentonite samples with different percentages of hematite. **a** Energy level 1173 keV. **b** Energy level 1332 keV

$\ln\frac{N_0}{N}$, which attenuates the rays passing through the sample. A summary of the results is presented in Table 3 to help investigate the effect of hematite powder on the performance of bentonite for protection against gamma radiation. Table 3 presents the values of linear attenuation coefficient in three laboratory methods, simulation with the MCNP code, and the XCOM database. The amount of laboratory measurement error was also determined by averaging between laboratory and simulation results. The information in the table shows that the simulation and laboratory results are in good agreement. It is also concluded that the linear attenuation coefficient increases with increasing the percentage of hematite powder. On the other hand, SEM images on BS, BSH15, BSH30, and BSH45 samples show that the particles have different structures; in other words, the bentonite particles are oval while the hematite powder particles are planar.

In addition to the radiation attenuation factor parameter, the hydraulic permeability parameter for radiation protection materials is imperative to consider. Hematite powder is one of the additives that as its amount increases in the mixture with bentonite, the hydraulic permeability coefficient will

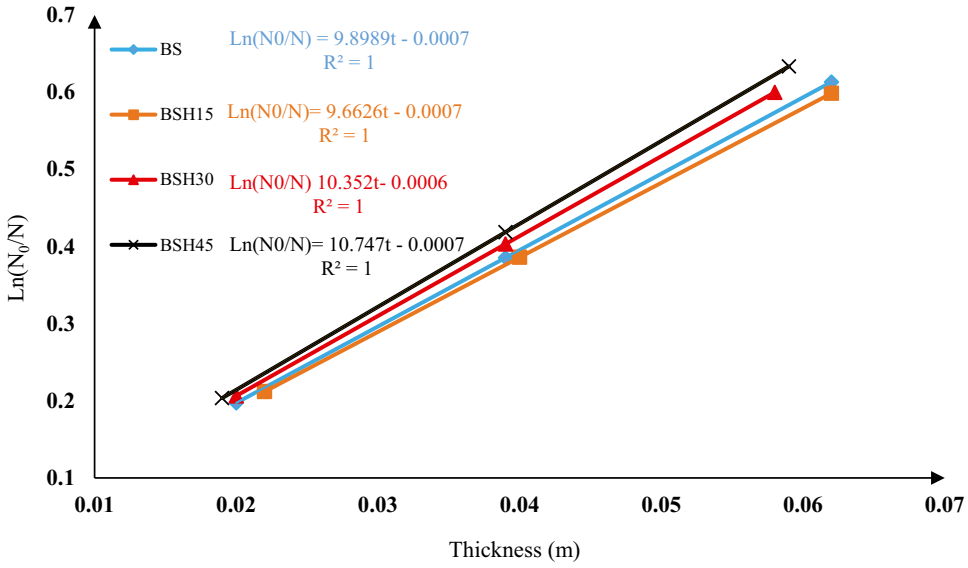

a) Energy level 1173 keV

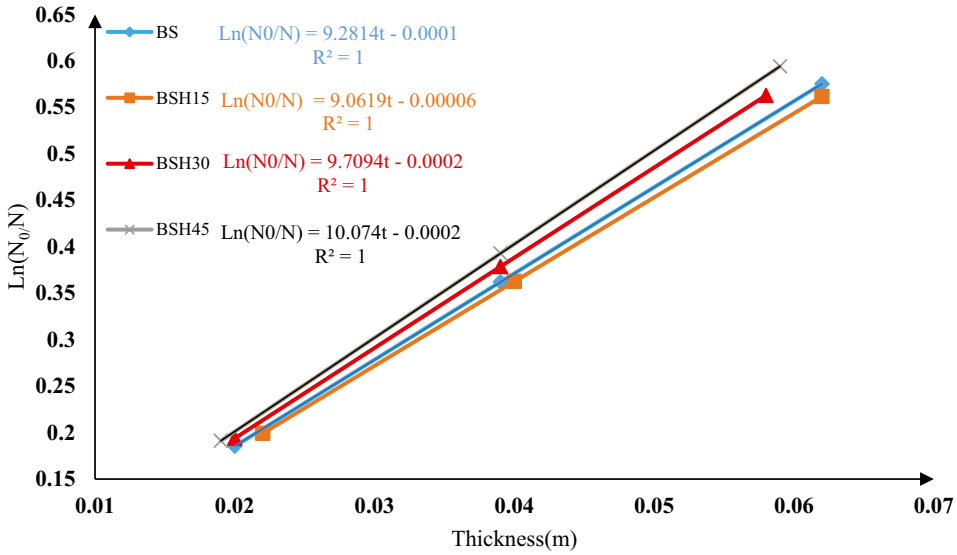

b) Energy level 1332 keV

Fig. 9 The variation of $\ln\frac{N_0}{N}$ against bentonite sample thickness with hematite powder in 1173 and 1332 energy levels using MCNP code. **a** Energy level 1173 keV. **b** Energy level 1332 keV

remain almost constant. However, this constancy in hydraulic permeability in the range of 15 to 45% of the additive was investigated. Due to the time-consuming permeability tests, the rate of increase in hematite powder is considered to be 15%. In general, the results presented in Fig. 12 indicate that a slight decrease in hydraulic permeability is observed by an increase in hematite powder percentage. This phenomenon can be explained by the lamellar structure of the hematite microscopic structure and the oval structure of bentonite, where under compaction the sheets are broken, filling the voids and blocking the water conductivity paths. Initially, adding hematite powder compared to pure bentonite shows a 27% reduction in hydraulic permeability. However, in a mixture with 30% and 45% hematite powder, the hydraulic permeability has increased by only about 3% compared to pure bentonite. In addition, the two samples BSH15 and BSH30 have almost the same permeability. The results show that the increase in hematite powder has a slight effect on the hydraulic permeability of the mixture, which could be very important.

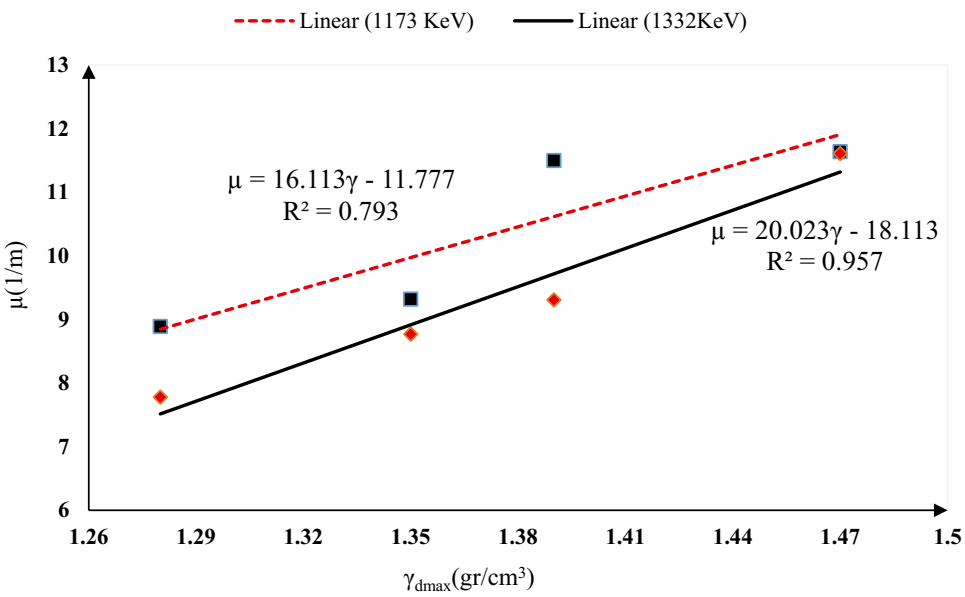

Fig. 10 Graph of the maximum dry unit weight versus linear attenuation coefficient for bentonite sample with hematite powder at different energy levels

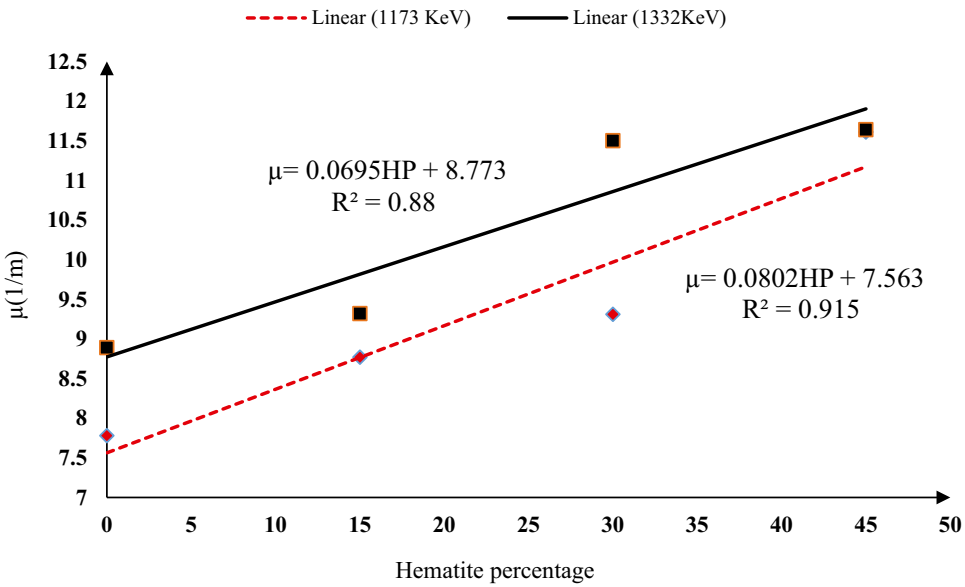

Fig. 11 Graph of linear attenuation coefficient versus percentage of hematite powder additive at different energy levels

Table 3 Results of linear attenuation coefficient obtained from laboratory data and modeling

Energy (keV)											
1332						1173					
TVL	HVL	XCOM	MCNP	Experimental		TVL	HVL	XCOM	MCNP	Experimental		Sample
				$\Delta\mu$	$\mu\,(^1/_m)$					$\Delta\mu$	$\mu\,(^1/_m)$	
0/3	0/089	9/28	9/28	0/19	7/78	0/26	0/078	9/9	9/89	0/11	8/89	BS
0/26	0/079	9/07	9/06	0/03	8/77	0/25	0/074	9/67	9/66	0/04	9/32	BSH15
0/2	0/06	9/7	9/7	0/04	9/31	0/2	0/06	10/3	10/35	0/11	11/5	BSH30
0/25	0/074	10	10/07	0/15	11/61	0/19	0/059	10/7	10/75	0/08	11/64	BSH45

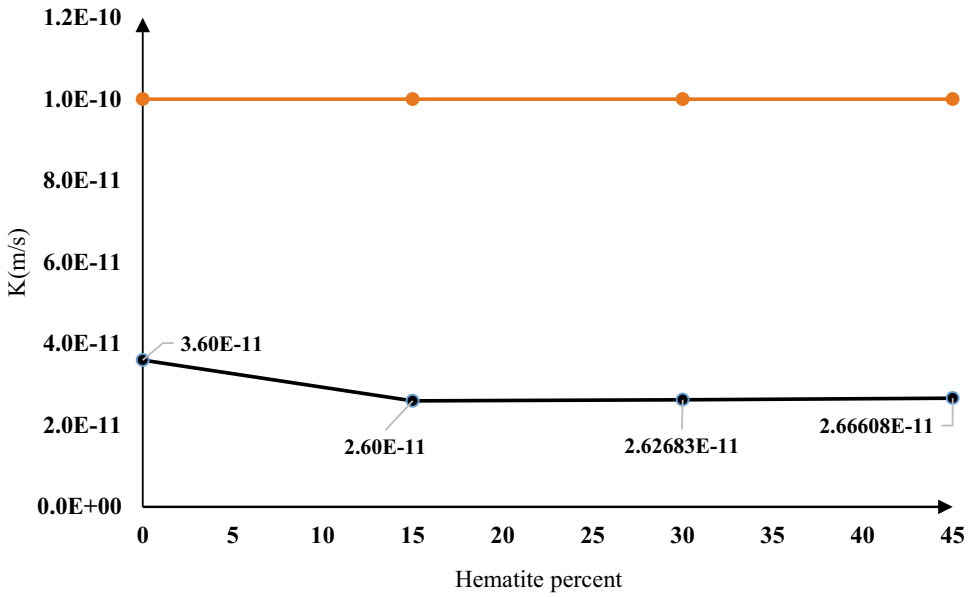

Fig. 12 Relationship between the hydraulic permeability versus different percentages of hematite additive

Conclusions

This study aimed to investigate the effect of hematite powder as an additive with 15, 30, and 45 percentages to sodium bentonite to improve the radiation shielding performance of landfill liners. For this, the linear attenuation coefficient is derived from three theoretical, simulation, and experimental methods for the sample mixtures and compared with pure bentonite. The hydraulic permeability is also assessed for the mixtures to ensure meeting the requirement of the EPA standard. Based on the study findings, the following were concluded.

- The radiation shielding performance is generally improved by increasing the hematite powder percentage in the mixture. This is due to the higher density of hematite powder compared to the bentonite resulting in higher radiation absorption.
- Based on the error analysis, the linear attenuation coefficient results obtained from the three approaches are in good agreement.
- The best radiation shielding performance was reached by bentonite with 45% of hematite power (BSH45). The linear attenuation coefficient of the sample at the energy levels of 1173 and 1332 was 11.64 and 11.61 m^{-1} from the laboratory tests, 10.75 and 10.07 m^{-1} from the MCNP simulation approach, and 10 and 10.7 m^{-1} from the XCOM database, respectively. This mixture provides 30 and 50% improvement in gamma-ray radiation shielding performance, at the energy levels of 1173 and 1332 keV, in comparison with the pure bentonite clay.
- Based on experimental measurements, the hydraulic permeability of the mixtures decreased almost 30% for pure bentonite to the mixture with 10% of hematite powder and stayed constant for more additive percentages. The hydraulic permeability for all mixtures was in the allowable range according to the EPA standard requirement.
- The results of the mixture with 45% of hematite powder reduce both TVL and HVL values by 25% and 17%, at the energy levels of 1173 and 1332 keV, respectively.

References

Abdo AES, Kansouh WA, Megahid RM (2002) Investigation of radiation attenuation properties for baryte concrete. Jpn J Appl Phys 41(12R):7512

Adegoke OS (1980) Guide to the non-metallic mineral industrial potential of Nigeria. Proceedings of the Raw Materials Research and Development Council 110–120

Agar O, Sayyed MI, Akman F, Tekin HO, Kaçal MR (2019) An extensive investigation on gamma ray shielding features of Pd/Ag-based alloys. Nucl Eng Technol 51(3):853–859

Akgün HA, Türkmenoğlu AG, Met İ, Yal GP, Koçkar MK (2017) The use of Ankara clay as a compacted clay liner for landfill sites. Clay Miner 52(3):391–412

Akkurt I, Canakci H (2011) Radiation attenuation of boron doped clay for 662, 1173 and 1332 keV gamma rays

Akman F, Khattari ZY, Kaçal MR, Sayyed MI, Afaneh F (2019a) The radiation shielding features for some silicide, boride and oxide types ceramics. Radiat Phys Chem 160:9–14

Akman F, Kaçal MR, Sayyed MI, Karataş HA (2019b) Study of gamma radiation attenuation properties of some selected ternary alloys. J Alloy Compd 782:315–322

Al-Ketan O (2012) Potential of using olive pomace as a source of renewable energy for electricity generation in the Kingdom of Jordan. J Renew Sustain Energ 4(6):063132

Alorfi HS, Hussein MA, Tijani SA (2020) The use of rocks in lieu of bricks and concrete as radiation shielding barriers at low gamma and nuclear medicine energies. Constr Build Mater 251:118908

Asal S, Erenturk SA, Haciyakupoglu S (2021) Bentonite based ceramic materials from a perspective of gamma-ray shielding: Preparation, characterization and performance evaluation. Nucl Eng Tech 53(5):1634–1641

Awadallah MI, Imran MM (2007) Experimental investigation of γ-ray attenuation in Jordanian building materials using HPGe-spectrometer. J Environ Radioact 94(3):129–136

Billen P, Leccisi E, Dastidar S, Li S, Lobaton L, Spatari S, Baxter JB (2019) Comparative evaluation of lead emissions and toxicity potential in the life cycle of lead halide perovskite photovoltaics. Energy 166:1089–1096

Bonaparte R, Beech JF, Griffin LM, Phillips DK, Kumthekar U, Reising J (2008) Design, construction, and performance of low-level radioactive waste disposal facility. Proceed 6th Int Conf Case Histories in Geotech Eng

Ceglie FG, Elshafie H, Verrastro V, Tittarelli F (2011) Evaluation of olive pomace and green waste composts as peat substitutes for organic tomato seedling production. Compost Science & Utilization 19(4):293–300

Ciaravella A, Scappini F, Franchi M, Cecchi-Pestellini C, Barbera M, Candia R, Micela G (2004) Role of clays in protecting adsorbed DNA against X-ray radiation. Int J Astrobiol 3(1):31–35

Cokca E, Yilmaz Z (2004) Use of rubber and bentonite added fly ash as a liner material. Waste Manage 24(2):153–164

Cui YJ (2017) On the hydro-mechanical behaviour of MX80 bentonite-based materials. J Rock Mech Geotech Eng 9(3):565–574

Damla N, Baltas H, Celik A, Kırıs E, Cevik UĞUR (2012) Calculation of radiation attenuation coefficients, effective atomic numbers and electron densities for some building materials. Radiat Prot Dosimetry 150(4):541–549

El-Sayed TA (2021) Performance of heavy weight concrete incorporating recycled rice straw ash as radiation shielding material. Prog Nucl Energy 135:103693

El-Sharkawy RM, Allam EA, El-Taher A, Elsaman R, Massoud EES, Mahmoud ME (2022) Synergistic effects on gamma-ray shielding by novel light-weight nanocomposite materials of bentonite containing nano Bi2O3 additive. Ceramics International 48(5):7291–7303

Elmahroug Y, Tellili B, Souga C (2014) Determination of shielding parameters for different types of resins. Ann Nucl Energy 63:619–623

Flora G, Gupta D, Tiwari A (2012) Toxicity of lead: a review with recent updates. Interdiscip Toxicol 5(2):47

Gencel O (2011) Physical and mechanical properties of concrete containing hematite as aggregates. Sci Eng Compos Mater 18(3):191–199

Gencel O, Ozel C, Filiz M (2011) Investigation on abrasive wear of concrete containing hematite

Isfahani HS, Abtahi SM, Roshanzamir MA, Shirani A, Hejazi SM (2019) Investigation on gamma-ray shielding and permeability of clay-steel slag mixture. Bull Eng Geol Environ 78(6):4589-4598

Kacal MR, Akman F, Sayyed MI (2019) Investigation of radiation shielding properties for some ceramics. Radiochimica Acta 107(2):179–191

Kaur S, Kaur A, Singh PS, Singh T (2016) Scope of Pb-Sn binary alloys as gamma rays shielding material. Prog Nucl Energy 93:277–286

Kavaz E (2019) An experimental study on gamma ray shielding features of lithium borate glasses doped with dolomite, hematite and goethite minerals. Radiat Phys Chem 160:112–123

Koch D (2002) Bentonites as a basic material for technical base liners and site encapsulation cut-off walls. Appl Clay Sci 21(1–2):1–11

Lansdown R, Yule W (1986) Lead toxicity: history and environmental impact. Johns Hopkins University Press

Lee SY, Tank RW (1985) Role of clays in the disposal of nuclear waste: a review. Appl Clay Sci 1(1–2):145–162

Lersow M, Waggitt P (2020) Disposal of all forms of radioactive waste and residues. Springer International Publishing

Levet A, Kavaz E, Özdemir Y (2020) An experimental study on the investigation of nuclear radiation shielding characteristics in iron-boron alloys. J Alloy Compd 819:152946

Li M, Zhang M, Du C, Chen Y (2020) Study on the spatial spillover effects of cement production on air pollution in China. Sci Total Environ 748:141421

Madi A, Kuraan L (1999) Jordan olive monthly report. Nat Centre Agricul Res Technol Trans Amman, Jordan

Mann HS, Brar GS, Mann KS, Mudahar GS (2016) Experimental investigation of clay fly ash bricks for gamma-ray shielding. Nucl Eng Technol 48(5):1230–1236

Mann KS, Singla J, Kumar V, Sidhu GS (2012) Verification of some building materials as gamma-ray shields. Radiat Prot Dosimetry 151(1):183–195

Mann KS, Rani A, Heer MS (2015) Shielding behaviors of some polymer and plastic materials for gamma-rays. Radiat Phys Chem 106:247–254

Mahmoud KA, Lacomme E, Sayyed MI, Özpolat ÖF, Tashlykov OL (2020) Investigation of the gamma ray shielding properties for polyvinyl chloride reinforced with chalcocite and hematite minerals. Heliyon 6(3):e03560

Nambiar S, Yeow JT (2012) Polymer-composite materials for radiation protection. ACS Appl Mater Interfaces 4(11):5717–5726

Nikbin IM, Mohebbi R, Dezhampanah S, Mehdipour S, Mohammadi R, Nejat T (2019) Gamma ray shielding properties of heavy-weight concrete containing Nano-TiO2. Radiat Phys Chem 162:157–167

Obaid SS, Sayyed MI, Gaikwad DK, Pawar PP (2018) Attenuation coefficients and exposure buildup factor of some rocks for gamma ray shielding applications. Radiat Phys Chem 148:86–94

Olukotun SF, Gbenu ST, Oladejo OF, Sayyed MI, Tajudin SM, Amosun AA, Fasasi MK (2020) Investigation of gamma ray shielding capability of fabricated clay-polyethylene composites using EGS5, XCOM and Phy-X/PSD. Radiat Phys Chem 177:109079

Oto B, Yıldız N, Akdemir F, Kavaz E (2015) Investigation of gamma radiation shielding properties of various ores. Prog Nucl Energy 85:391–403

Omotoyinbo JA, Oluwole OO (2008) Working properties of some selected refractory clay deposits in South Western Nigeria

Pusch R, Hatem M, Kasbohm J, Knutsson S (2013) Roles of clay and concrete in isolating high-level radioactive waste in very long holes. Int J Res Rev Appl Sci 16(2):263–273

Poltabtim W, Wimolmala E, Saenboonruang K (2018) Properties of lead-free gamma-ray shielding materials from metal oxide/EPDM rubber composites. Radiat Phys Chem 153:1–9

Rahman RRO, Ibrahium HA, Hung YT (2011) Liquid radioactive wastes treatment: a review. Water 3(2):551–565

Ristinah S, Wisnumurti N, Djakfar L (2011) Evaluation of the characteristic of heavyweight concrete using steel slag aggregates for radiation shielding. J Appl Environ Biol Sci Brawijaya, Indonesia 1(11):512–521

Saling J (2001) Radioactive waste management. CRC Press

Singh T, Kaur A, Sharma J, Singh PS (2018a) Gamma rays' shielding parameters for some Pb-Cu binary alloys. Eng Sci Technol Int J 21(5):1078–1085

Singh J, Singh H, Sharma J, Singh T, Singh PS (2018b) Fusible alloys: a potential candidate for gamma rays shield design. Prog Nucl Energy 106:387–395

Singh R, Singh S, Singh G, Thind KS (2017) Gamma radiation shielding properties of steel and iron slags. New J Glass Ceram 7(01):1

Swiss Standard SN (1999) 670 010b. Characteristic coefficients of soils, association of Swiss road and traffic engineers

Uwasu M, Hara K, Yabar H (2014) World cement production and environmental implications. Environ Develop 10:36–47

Wani AL, Ara A, Usmani JA (2015) Lead toxicity: a review. Interdiscip Toxicol 8(2):55

XCOM N (2010) Element/compound/mixture-physical measurement. Nat Instit Standard Technol

Yue K, Luo W, Dong X, Wang C, Wu G, Jiang M, Zha Y (2009) A new lead-free radiation shielding material for radiotherapy. Radiat Prot Dosimetry 133(4):256–260